Roles of Boiling Surface Characterized by Micro-structures on Boiling Heat Transfer and Critical Heat Flux

Seol Ha Kim, Jun Young Kang, Moriyama Kiyofumi, Hyun Sun Park*, and Moo Hwan Kim
Division of Advanced Nuclear Engineering, POSTECH
Pohang, 790-784, Republic of Korea
findys@postech.ac.kr; kkang0620@postech.ac.kr; khmoriyama@postech.ac.kr,
hejsunny@postech.ac.kr, mhkim@postech.ac.kr

Gi Cheol Lee
Department of Mechanical Engineering
POSTECH
Pohang, 790-784, Republic of Korea
chol4459@postech.ac.kr

ABSTRACT

As one of a key phenomenon in nuclear reactor thermal hydraulics, nucleate boiling has been widely studied by numerous researchers to improve plant design efficiency and safety. In general, the evaluation of the boiling performance mainly focus on two physical parameters: boiling heat transfer (BHT) and critical heat flux (CHF). In the nuclear power plants, since both BHT and CHF contribute the nuclear system efficiency and safety, respectively many new approaches to enhance the boiling performance compared to the conventional methodology have been investigated. Recently new progress in micro-nano manufacturing techniques has been made and enables to fabricate the precisely engineered boiling heating surface. The new techniques even allows to develop advanced boiling models by observing the fundamental phenomenology associated in boiling process by controlling the specific surface characteristics that includes cavity configuration, surface wetting conditions, etc.

We recently focused on the implications and limitation of the microstructured surface on the enhancement of the boiling performance (BHT & CHF). We designed a set of experiments that prepare 13 samples; the 12 samples of microstructured surfaces and one bare surface has been fabricated by MEMS (Micro Electro Mechanical Systems) techniques. The samples was tested for the pool boiling experiments at saturated and atmospheric pressure conditions. For BHT, the experimental results show that BHT increases with the surface roughness defined as the ratio of the actual area to the projected area but the enhancement gradually slows. Overall, the heat transfer coefficient of the structured surfaces increases more than 300% compared to that of the bare surface. The increase of the heating surface area with the roughness ratio improves nucleate boiling heat transfer due to the enhancement of convective heat transfer. For CHF, the structured surfaces shows up to 350% enhancement with respect to that of the bare surface. However In the analyzing the capillary flow rate on the structured surface it is found that the critical size (gap) that limits the CHF enhancement exists. In this study, the critical size has been analytically discussed and compared with experimental data. Based on the above understanding role of the microstructured surface on both BHT and CHF found in our study, the optimal design of boiling performance (HTC & CHF) can be suggested.

KEYWORDS
Boiling Heat Transfer, Critical Heat Flux, Microstructure Surface

1. INTRODUCTION

As one of a key phenomenon in nuclear reactor thermal hydraulics, nucleate boiling has been widely studied by numerous researchers to improve plant design efficiency and safety. In general, the evaluation of the boiling performance mainly focus on two physical parameters: boiling heat transfer (BHT) and critical heat flux (CHF). In the nuclear power plants, both BHT and CHF contribute the nuclear system efficiency and safety, respectively. Due to its importance in not only nuclear thermal hydraulics but also other thermal manage system, numerous study has been carried out. From fundamental study to high technique based performance enhancing study of the pool boiling has been reported.

For decades, nucleate-boiling heat transfer has been predominantly an empirical science, accompanied by relatively simple models based on hypotheses that are not always fully justified. For example, the widely popular Rohsenow's correlation [1] for nucleate boiling is based on the assumption that single-phase convection and nucleate boiling are analogous physical processes. In recent, the more mechanistic model of nucleate boiling heat transfer has been developed, [2] considering the bubble behaviors of boiling. By observing and measuring boiling parameters (bubble size, bubble frequency and nucleate site density), semi-empirical model boiling heat transfer, such as the heat flux partitioning model, was presented. According to the above partitioning model, three kinds of sub-mechanism for heat transfer by boiling bubble are described. Here, each heat transfer contribution comes from convective effect by bubble agitation, transition re-heating within thermal boundary layer after bubble releasing and evaporation of latent heat during bubble growth. In classical, CHF has traditionally been attributed to a surface-independent hydrodynamic mechanism associated with the Kelvin–Helmholtz instability. [3,4] Over the last decade, several trials, in addition to Zuber's hydrodynamic model, have been used to interpret the CHF phenomena. Then, the introduction of a thin liquid layer, or macrolayer, beneath a large bubble growth, is postulated to induce vaporization of the entire macrolayer by heat flux from the heated surface within the bubble cycle, triggering the CHF phenomena. [5,6] In recently, the more surface dependent analysis has been studied and its experimental observation has been reported.

Recently new progress in micro-nano manufacturing techniques has been made and enables to fabricate the precisely engineered boiling heating surface. The new techniques even allows to develop advanced boiling models by observing the fundamental phenomenology associated in boiling process by controlling the specific surface characteristics that includes cavity configuration, surface wetting conditions, etc. From 2000s, nanofluids has widely been adopted to enhance CHF with its capillary wicking effect. Kim et al. [7], You et al. [8], and Bang et al. [9] reported the CHF enhancement through the nanofluid pool boiling experiments, and they figured out that the deposited nanoparticle contribute the capillary wicking effect on to CHF increment. Recently, nanostructured surface also has been evaluated in not only CHF and BHT increment. Chen et al. [10] reported the silicon nanowire contribute CHF enhancement by modulating instability and BHT increase. Jo et al. [11] also reported both CHF and BHT increment on nano-scaled silicon structure surface. During the pool boiling experiments, smaller but many nucleated bubble behaviors has been observed, and it contributed the BHT increment. Above nano scaled particle or structured surface shows irregular geometric morphology on the boiling surface. On the other hand, nowdays regular morphology of microscaled structured surface has been developed and evaluated in boiling performance. Liter and Kaviany [12] performed CHF increment on sphere (60~200um) particle based porous surface. They analyzed the role of porous medium as a capillary wicking effect driving, and reported the CHF increment. Kandlikar [13] reported that the several hundreds of micro structure of heating surface triggered bubble motion during the pool boiling, and it shows tremendous boiling heat transfer enhancement. Chu et al. [14] utilized well-defined silicon micropillar arrays to demonstrate the role of surface roughness for CHF enhancement. Their proposed CHF model, based on the roughness-amplified capillary forces pinning the contact line of the vapor bubble, showed good agreement with experimental data.

According to the above many reports, boiling performance (BHT and CHF) has been evaluated on various micro/nano scaled structure surface. However, the role of nano/micro structured surface on pool boiling has not been established in clearly. Each experimental observation and their analysis shows slight different trend and results. The basic understanding of the role of the nano/micro structures surface give us fundamental insight of the boiling performance (CHF and BHT) and it directly contribute the nuclear thermal hydraulics system (safety and efficiency). In order to figure out that, systematic approach from designing structure surface to experimental analysis should be supported. In this study, BHT and CHF of the pool boiling on well-organized fabricated structured (micro scaled) surface has been evaluated. As a results, BHT change on microstructured surface shows strongly dependent on Pin-fin effect analysis. In terms of CHF, critical size of micro structure for CHF enhancement has been observed and analyzed based on the capillary wicking effect. Finally, this study can contribute the basic understanding of the boiling on designed microstructure surface, and it also suggest the optimal micro scaled structured surface of boiling performance.

2. Experiment

2.1. Sample Preparation

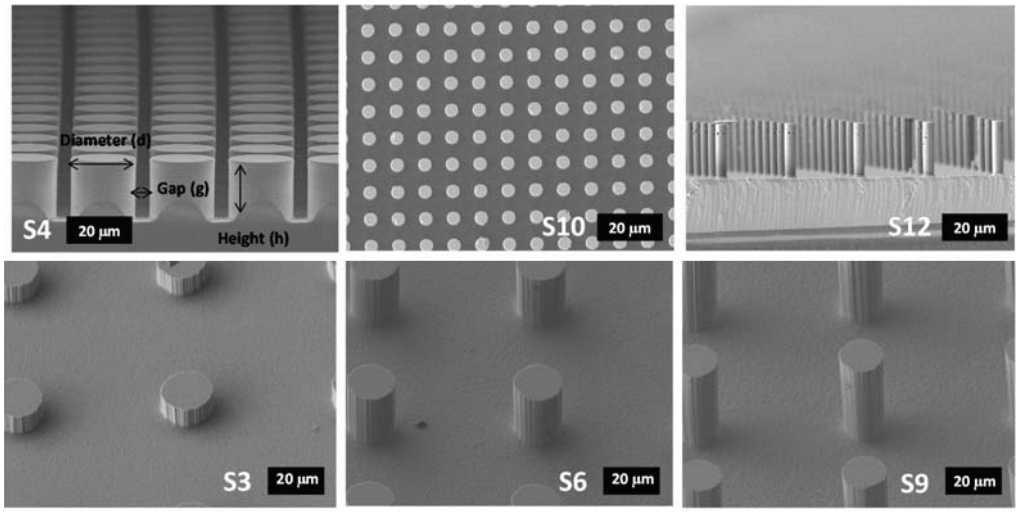

Figure 1. Sample Figure.

Table I. Geometric properties of the microstructured sample surfaces

Sample No.	d	h	g	Roughness (r)	Solid Fraction
S0	-	-	0	1	1
S01 (D20H10G05)	20	10	05	2.00	0.50
S02 (D20H10G20)	20	10	20	1.39	0.20
S03 (D20H10G40)	20	10	40	1.17	0.09
S04 (D20H20G05)	20	20	05	3.01	0.50
S05 (D20H20G20)	20	20	20	1.79	0.20
S06 (D20H20G40)	20	20	40	1.35	0.09
S07 (D20H40G05)	20	40	05	5.02	0.50
S08 (D20H40G20)	20	40	20	2.57	0.20
S09 (D20H40G40)	20	40	40	1.70	0.09
S10 (D05H20G05)	05	20	05	4.14	0.20
S11 (D05H20G10)	05	20	10	2.40	0.09
S12 (D05H20G20)	05	20	20	1.50	0.03

Figure 1 shows scanning electron microscopy (SEM) images of representative microstructures used in this study. Table 1 lists the geometric features of the prepared samples (nine structured cases and one bare case). The circular-micro pillar arrays were etched in silicon using deep reactive ion etching (DRIE), with a roughness r, defined as the ratio of the actual area in contact with the liquid to the projected area; the roughness ranged from 1.00 to 4.4. Several length scales (5~40 μm) were designed as geometric parameters (i.e., height, diameter, and gap). A 120-nm-thick platinum (Pt) layer was deposited on the back side of the samples to facilitate attachment by soldering to the experimental setup. Using an electrical joule-heating method with the Pt layer, the power input (heat flux) and heating temperature were measured. For all of the tests, the samples were degassed (saturated condition) for 2 h; additionally, high purity water was used to avoid premature bubble formation and to minimize surface contamination. All of the samples were tested two to three times to check for consistency.

2.2. Experimental Setup

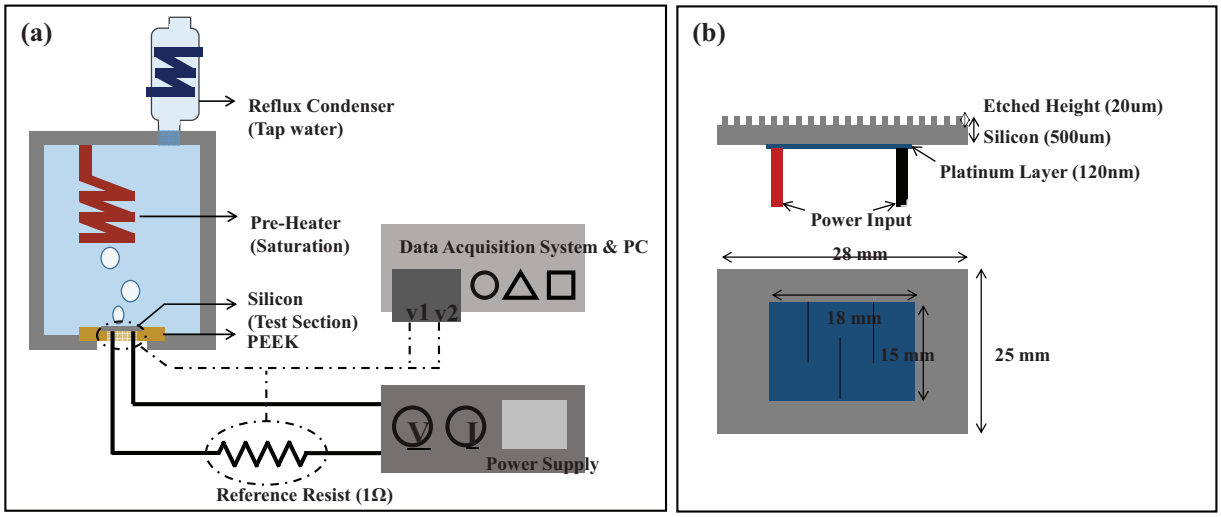

Figure 2. Sample Figure. (a: Pool Boiling Experimental Setup, b: Test Section)

In this study, a pool boiling experiments was carried out as shown Fig. 2. The facility was composed of a test sample jig, a main test pool and a lid with an immersion heater (pre-heater) and condenser. The pre-heater applies heat to D.I. water pool for 2 hours before main experiments. During the two hours, dissolved gas in the water pool would be degassed and saturated condition would be maintained, and the condenser keep a water level by tap water cooling. The test sample jig consisted of a PEEK (polyetheretherketone) test sample frame and silicon test sample. PEEK is a thermoplastic that has high thermal resistance and is compatible with an aqueous environment. The test samples were fixed with adhesive binary epoxy (DuralcoTM 4365). The test sample was heated electrically using a platinum (Pt) electrode, which was deposited on the bottom surface of the silicon wafer. (Fig. 2) Electrical power was supplied using a Sorensen DLM 300-13E power supply. A data acquisition system (Agilent 34970A) was used to measure the input power (heat flux) and a temperature of the Pt electrode, which is considered as Temperature of wall (T_{wall}). As direct monitoring the two voltage value of test section and reference resistance, the circuit current (I_{cir}) and resistance of Pt heater (R_{heat}) were calculated. Finally, the heat flux was calculated from the above electrical quantities and test sample heater area (A_{heat}). And, the wall temperature (T_{wall}) also was calculated using the measured R_{heat} from operation and calibration data (Temperature – R_{heat}) for each sample. Considering all the instrument errors, the maximum uncertainties of heat flux and wall super heat were estimated about 9.03 kW/m^2, 4.44℃, respectively.

3. Results

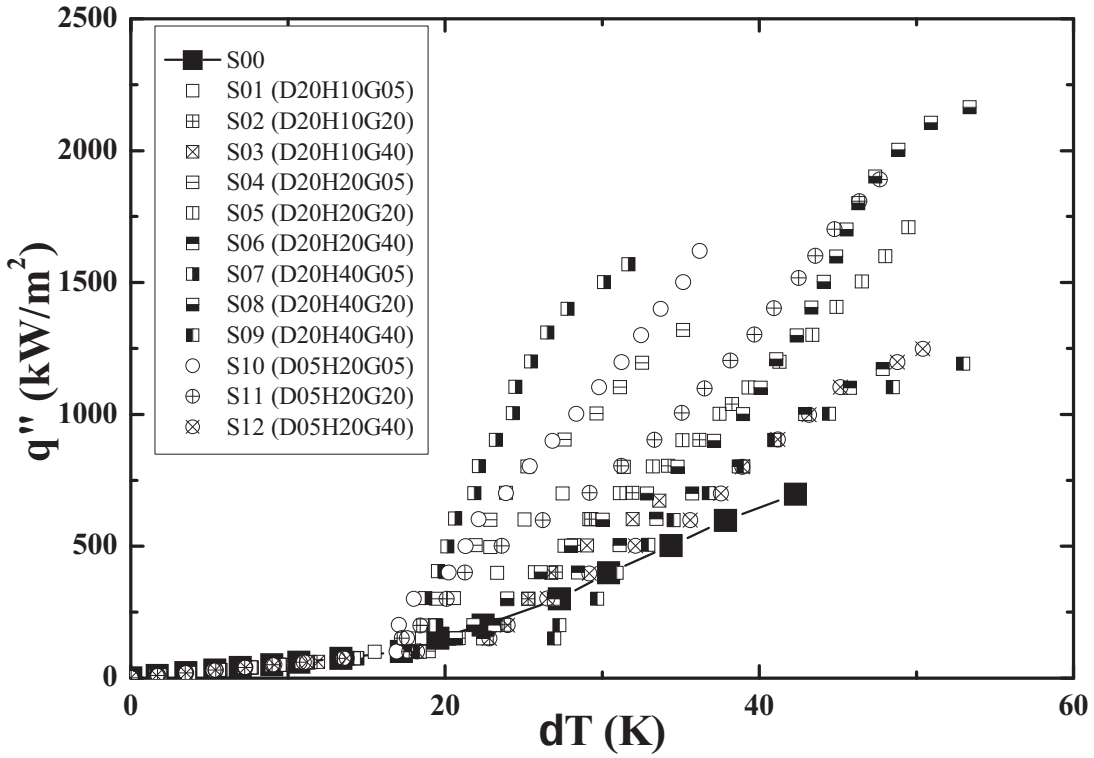

Figure 3. Boiling curve

Figure 3 shows the boiling experimental results on the smooth Si surface (S0) and microstructured surfaces (S1–S12). The performance plot of the heat flux q" as a function of the wall super heat $\Delta T=T_w-T_{sat}$, where Tw is the heated surface temperature and T_{sat} is the saturation temperature, is shown for all cases; the data in Fig. 3 represent the average obtained from two to three rounds of experimental testing (four times for the smooth surface case, S0). The maximum uncertainties in the heat flux and temperature measurements were approximately 6.3% and 2.8 K, respectively. In general, the boiling curves indicated that the structured surfaces (S1–S12) experienced significantly enhanced boiling heat transfer (as evidenced by the slope of the boiling curve) and CHF (heat flux at the end point), compared with the smooth surface (S0). At low super heat regime (before the onset of nucleate boiling, ONB), the boiling heat transfer of the prepared surfaces has no difference. However, after ONB, the boiling heat transfer on structured surface becomes much higher performance compared to the bare surface. Although there are several delayed ONB point on the structured surface, BHT at fully developed nucleate boiling regime (~30K) or near CHF on the structured surface shows higher that on the Bare surface. Its trends along the structured surface would be discussed later chapters. In terms of CHF, the bare smooth surface (S0) exhibited a heat flux of 697.8 ± 44.1 kW m−2 at 42.3 ± 2.8 K, and the S08 case achieved the highest CHF performance with 2165 kW m−2 at 53.39 K (3100% that of the S0 case). Note that S07 had the highest surface roughness; its CHF performance was 1569 kW m−2 at 31.67 K, which was less than both S08 and S09 (both with smaller surface roughness than S07). Additionally, the wall superheat points in S1 were also lower than the other two cases. These experimental results differ from those presented in a previous study that reported a CHF increase with the surface roughness. [14] The physical reasons for this and an interpretation of the experimental observations will be discussed later in the text.

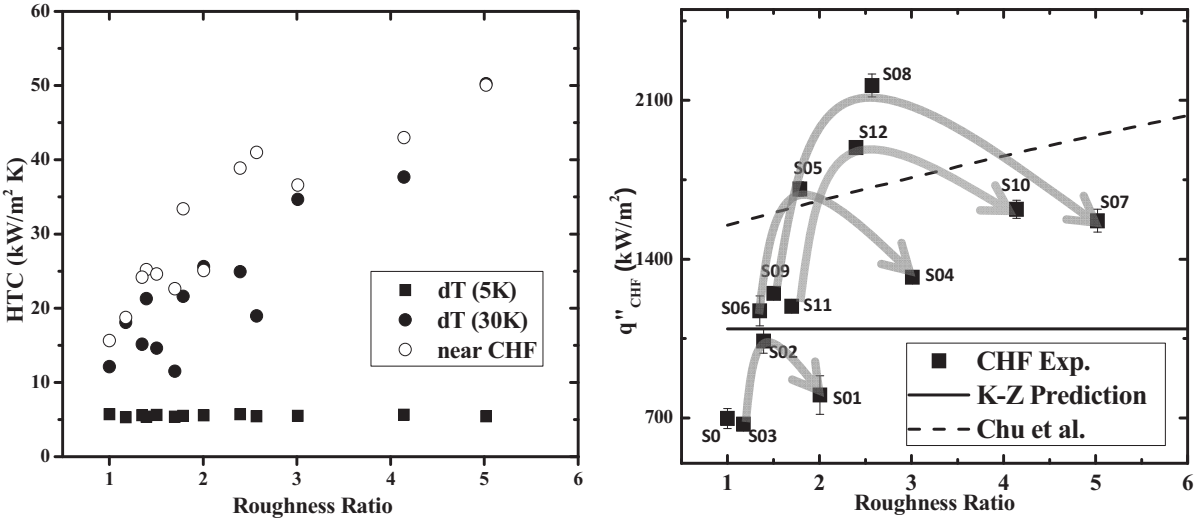

Figure 4. Boiling performance trend along roughness ratio

Figure 4 (a,b) shows the BHT and CHF results of the test samples as a function of the surface roughness factor, respectively. The roughness factor is defined as an area fraction between actual value and projected value. According to the Fig. 4 (a), the Heat Transfer Coefficient (HTC) shows dependency on the roughness factor at high super heat regime and CHF. However, the low super heat regime (before ONB) shows no dependency on samples roughness. Since there no bubble generation before the ONB, only natural convection dominate the heat transfer rate. And, the thermal boundary layer (~100um) of the natural convection regime is higher than the structures height (10~40um) on the heating surface, so the structure couldn't affect the heat transfer rate. However, after ONB, the nucleated bubble behaviors strengthen convective effect, and it affect the thermal boundary layer. Due to the enhanced convective effect on the heating surface by bubble dynamics, the higher heat transfer rate can be obtained from the structured surface with roughness ratio. It is directly related with Fin effect, and would be quantitatively discussed in the next chapter. In Fig. 4(b), solid and dashed lines indicate the CHF prediction from the hydrodynamic instability analysis (Kutateladze–Zuber analysis) and the roughness-capillary effect analysis (Chu et al., 2012), respectively. Because the hydrodynamic instability analysis does not reflect the surface conditions (e.g., wetting and roughness), its prediction is independent of the change in roughness. On the contrary, the roughness-capillary effect analysis and present experimental CHF data generally show an increasing trend with increase in roughness. However, from our data, the S01, S04, S07 and S10 cases with higher roughness values exhibited lower CHF values than S02, S05, S8 and S11 with lower roughness values, respectively. Among those, Samples S01–S03 had the same diameter (20 μm); however, the gap spacing ranged from 5 μm (for S01) to 40 μm (for S03). As the gap between the micropillars decreased (i.e., the roughness increased), the CHF value increased from S03 to S02, but decreased from S02 to S01. This CHF oscillatory tendency (i.e., ups and downs with roughness or changes in the gap) was also observed for Samples S04–S06, S07-S09 and S10-S12; these three samples had the same diameter (20 μm) and different gaps (ranging from 5– 40 μm); here, the CHF also showed an oscillatory trend with changes in the gap. In principle, as the spacing between the micropillars decreases, the roughness factor increases due to an enlarged wetted surface area. Furthermore, the enhanced roughness increased the capillary force of the liquid rewetting the dry bubble patch, resulting in a CHF delay. However, the above experimental results imply that the capillary effects amplified by surface roughness should be limited by a certain critical size of the gap (spacing). Here, we suggest that the liquid in-flow performance, which is directly related to the rewetting capability of the dry patch, decreases with changes in the gap size, due to the reduced permeability of the microstructured surface.

4. Discussion

4.1. Boiling Heat Transfer Analysis

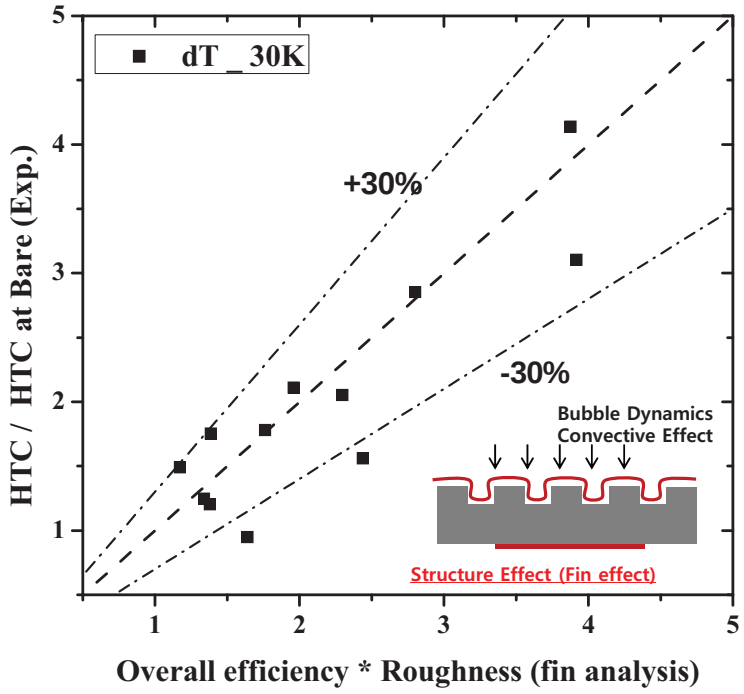

Figure 5. Pin fin analysis

According to the BHT results from the previous chapter, BHT on structured surface shows roughness dependency. The extended heat transfer area by roughness ratio contribute the heat transfer increase. The fin effect of the structured surface can account for the quantitative analysis of the BHT enhancement. As assuming the single phase convective heat transfer, the effect of the extended area by micro pillars would be calculated. In this study, the structures are array of circular micro pillar. It can be descried with the "Pin-fin analysis" and its fin efficiency (η) shows followings [15];

$$\eta = \frac{\tanh mh_c}{mh_c} \tag{1}$$

where $m^2 = h_{HTC}P/kA_c$ and $h_c = h + (d/4)$. The fin efficiency is defined as a ratio between fin heat transfer and maximum heat transfer rate, so the value indicates the fraction of the actual heat transfer among the maximum (ideal) heat transfer (always smaller than 1).
In addition, the structures surface has not a single fin but array of multiple fins. In case of the multiple fins, the total heat transfer can be described by the followings;

$$q_t = N\eta h_{HTC} A_f \Delta T + h_{HTC} A_b \Delta T \tag{2}$$

where N is the number of fin and A is area. 1st term of the RHS indicate the heat transfer by pin-fin and 2nd term shows the heat transfer from base surface. Then, the equation (2) will be simplified with the following procedure. First, by distributive law with the heat transfer coefficient (h) and wall super heat (ΔT), the equation is expressed;

$$q_t = h_{HTC}\left[N\eta_f A_f + \left(A_t - NA_f\right)\right]\Delta T \quad (3)$$

The area terms (fin side and base side) in the square bracket would be replaced by total area (A_t) with a several relation. Then, the total area can be extracted from the bracket, and the bracket becomes non-dimensional.

$$q_t = h_{HTC}A_t\left[1-\frac{NA_f}{A_t}\left(1-\eta_f\right)\right]\Delta T \quad (4)$$

The inside term of a square bracket defined the overall fin efficiency (η_o) of the multiple fin array surface. Then, the total area (A_t) can be expressed by the multiplication between base area and roughness. Finally, the total heat transfer on the structured surface can be described by fin analysis;

$$q_t = h_{HTC}A\cdot\left(r\cdot\eta_o\right)\Delta T \quad (5)$$

According to the above heat transfer rate relation, the heat transfer performance evaluation between structured surface and bare surface can be described by the multiplication between roughness and overall efficiency.

$$\frac{h_{HTC\_str}}{h_{HTC\_bare}} = r\cdot\eta_o \quad (6)$$

Figure 5 shows the heat transfer coefficient comparison between structured samples and bare sample, and it shows good agreement with the above fin analysis results (30% of error).

4.2. Critical Heat Flux Analysis

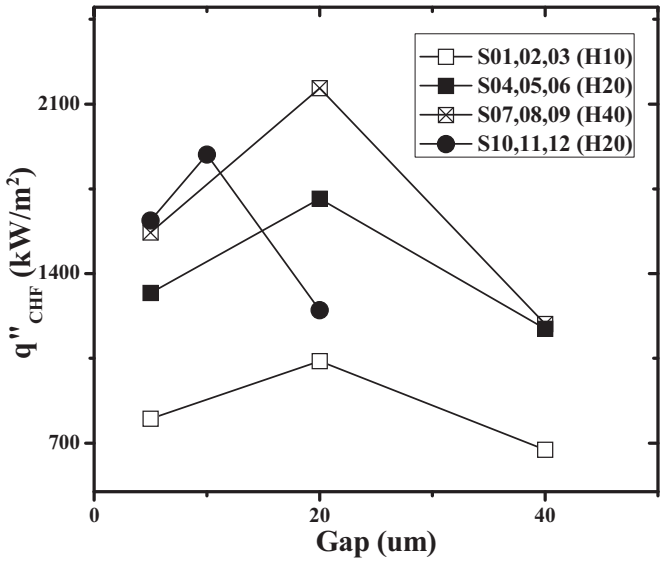

Figure 6. CHF change depending on gap

According to the CHF results from the previous chapter, CHF on structured surface shows not only enhancement but also oscillating behavior along the micro pillar gap size. It indicate that there is an optimal gap size for the CHF enhancement. Figure 6 shows the CHF trend depending on gap of the micro pillars. First, the pillar height generally affect the CHF enhancement. In this study, the prepared samples shows

pillar height dependency for the CHF performance. Then, the critical size of the gap is clearly observed, and the optimal trend would be explained.

First of all, we assumed that the higher liquid inflow during rewetting improves cooling on a dry/hot spot, the higher permeable liquid inflow rate through the structured surface (assumed as a porous medium) is desirable for CHF delay. During the rewetting process of the dry patch, the liquid inflow rate is triggered by the capillary wicking phenomena, due to the microscale small gaps in the structured surface. However, the apparent liquid inflow rate is limited by the permeability of the porous medium to the capillary intake flow rate. (See Figure 5) In other words, in order to make the capillary effect on the CHF delay apparent, even the capillary force on liquid-vapor interface increases due to a small gap, since the permeable flow rate has to be satisfied with the capillary-induced liquid flow rate. In general, the smaller gap (g, pore) improves the capillary pressure ($\Delta P_{cap} \propto 1/g$) on liquid in-flow, in addition to the friction of the porous layer. Here, both the capillary-induced flow rate and the permeable flow rate are modeled to predict the critical size of structures for the enhancement of CHF. First, the capillary pressure induces liquid inflow by structures:

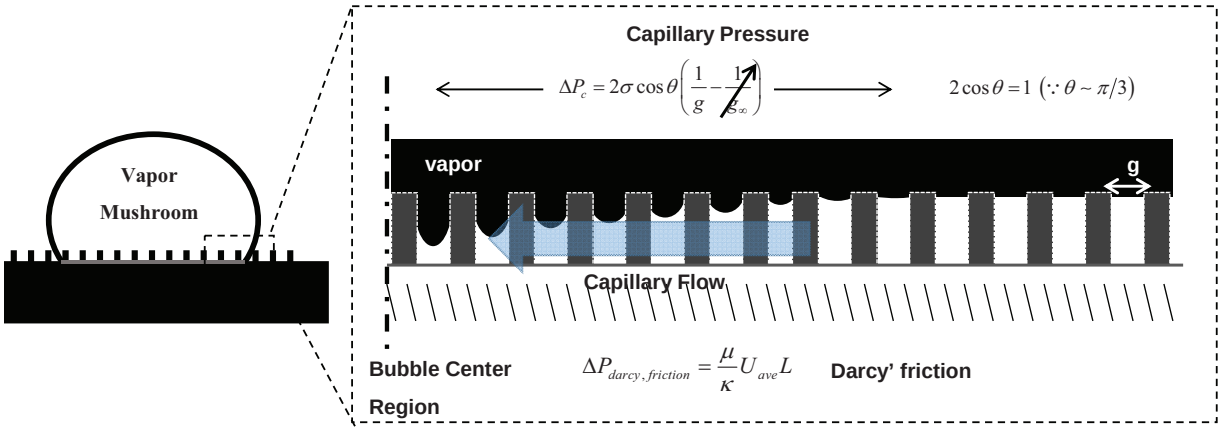

Figure 7. Capillary Liquid Inflow Rate Modelling

In order to evaluate the induced capillary flow rate, the above two relations (capillary pressure force and Darcy frictional pressure drop) would be modelled followings;

$$\frac{2\sigma\cos\theta_Y}{g} - \frac{\mu}{\kappa} u_{ave} L = \frac{1}{2}\rho u_{ave}^2 \tag{7}$$

The first term in left side hand is capillary driven momentum (where σ is the surface tension, and θ_Y is the contact angle), and the second term is friction loss (where κ is the permeability, μ is the dynamic viscosity of the liquid). Here, the capillary-induced liquid inflow passes through the micropillar arrays, the Carman-Kozeny permeability relationship ($K = d^2\varepsilon^3/16CK(1-\varepsilon^2)$) has been used. [16] Also, the porosity of the structured surface is ($\varepsilon = 1 - \pi d^2/4(d+g)^2$), where d is the diameter of the micropillar.The right hand side is the apparent inertia of the induced flow, results from the momentum balance between capillary pressure and friction. The Eq. (6) has second order of averaged velocity, and its solution can be obtained easily followings;

$$u_{ave} = -\frac{L}{\kappa}\frac{\mu}{\rho} + \sqrt{\left(\frac{L}{\kappa}\frac{\mu}{\rho}\right)^2 + \frac{1}{2g}\frac{\sigma}{\rho}} \tag{8}$$

The Eq. (7), averaged liquid inflow velocity is affected by several liquid properties and geometric parameter of micro structure. Gap between pillars affect the capillary pressure and permeability, and the diameter affect the permeability. The geometry shape and its arrangement affect the permeability modelling. (Detail modelling of the permeability would be discussed in the later works, not the scope of this article) The characteristic length (L) of the liquid flow also affect the pressure loss gradient, and it affects the flow rate. The averaged liquid inflow rate directly affect the CHF increment, and the larger inflow rate the higher CHF increment.

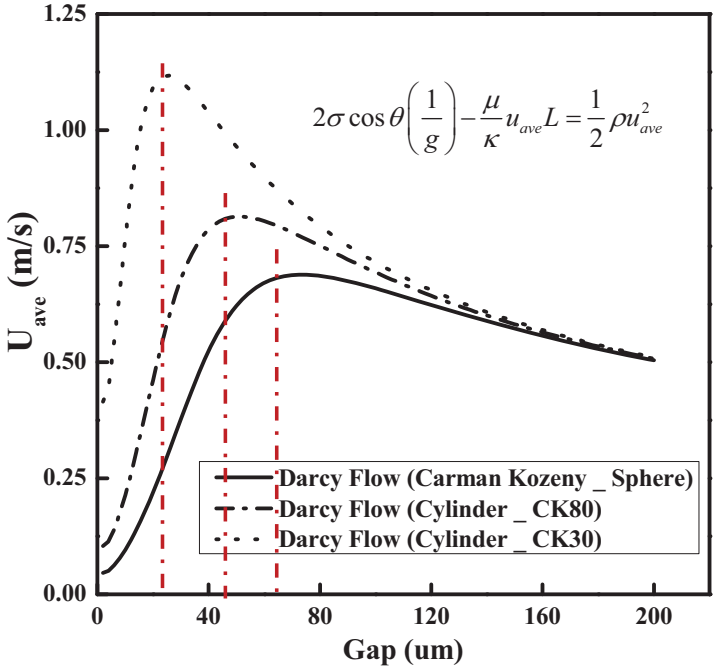

Figure 8. Capillary Liquid Inflow rate along the gap

Figure 8 describes the capillary induced liquid inflow velocity (Eq. 7) with respect to gap (spacing between micropillars). The inflow velocity shows optimal behavior depending on several Carman-Kozeny constant which directly affect the permeability. Here, the characteristic length (L) has been assumed for 100um. The optimal point depending on the CK constant, and its critical size of gap indicate 20~60μm. As the gap become smaller than optimal point, the inflow velocity sharply decrease due to the enlarged friction. In addition, the gap becomes larger than optimal point, the inflow also gradually decrease due to the lower capillary pressure. We assumed that the inflow rate directly affect the CHF increment on the structured surface. Rewetting capability of dryout near CHF condition is directly affected by capillary induced inflow, and its amount is able to delay CHF. This capillary induced flow velocity shows optimal points analytically, and its effect to CHF increment also can be observed from the experimental results (Figure 6). This capillary limit analysis of the CHF change is in good agreement with our experimental results. In Fig. 6, the CHF value decreased with the gap size change from 20 to 5 μm (i.e., S2 > S1, S5 > S4, and S8 > S7). Additionally, for the group of samples of the same gap size (S1, S4, and S7), the higher roughness conditions showed a higher CHF value, as observed in a previous study. As mentioned above, the narrower gap between micropillars creates more friction to liquid flow, resulting in a reduction in the capillary effect. Thus, it is expected that if the gap size becomes infinitely narrow (i.e., approaches zero), then liquid inflow to rewet the dry patch by the capillary effect is prevented. Thus, the CHF performance may approach that observed for the smooth bare surface as the gap diminishes.

5. Conclusion

In this study, BHT and CHF of the pool boiling on well-organized fabricated structured (micro scaled) surface has been evaluated. As a results, BHT change on microstructured surface shows strongly dependent on Pin-fin effect analysis. The extended heat transfer area contribute the boiling heat transfer increase on the structured surface, and its quantitative analysis has been performed. Within 30% of the heat transfer coefficient from the pin fin analysis, the experimental results shows good agreement.

In terms of CHF, critical size of micro structure for CHF enhancement has been observed and analyzed based on the capillary wicking effect. We suggested a capillary limit to CHF delay for modeling capillary induced liquid inflow through microstructured surfaces. The critical size of the capillary limit on the prepared structured surface, determined through modeling, could be reasonable explanation points for the experimental results (optimal size for CHF delay). The geometric parameters of the gap and microstructured surfaces played two important roles with respect to liquid in-flow. The smaller gap improved the capillary wicking rate, which triggered the liquid inflow rate, while the smaller gap reduced the permeable liquid inflow, which became apparent in rewetting situations. The present experimental results also showed clearly the critical size (10 ~ 20μm) for CHF delay, predicted by capillary limit analysis.

This study provides fundamental insight into BHT and CHF enhancement of structured surfaces, and an optimal design guide for the required CHF and boiling heat-transfer performance. Finally, this study can contribute the basic understanding of the boiling on designed microstructure surface, and it also suggest the optimal micro scaled structured surface of boiling performance. Additionally, the study contributes to new surface technologies with high heat-removal capabilities for not only nuclear thermal hydraulics but also other advanced thermal management applications.

NOMENCLATURE (IF NEEDED)

d	diameter of micro pillar	[m]
g	gap of micro pillars	[m]
h	height of micro pillar	[m]
r	roughness ratio	[-]
η	fin efficiency	[-]
h_{HTC}	heat transfer coefficient	[kW/m^2K]
P	perimeter of micro pillar	[m]
k	thermal conductivity of micro pillar	[W/mK]
A	area	[m^2]
N	number of micro pillar	[#]
σ	surface tension	[N/m]
θ	contact angle	[°]
μ	viscosity of liquid	[Pa s]
κ	permeability	[-]
ρ	density of liquid	[kg/m^3]
u	velocity	[m/s]
ε	porosity	[-]
CK	Carman-Kozeny Constant	[-]
L	characteristic length of liquid flow	[m]

Subscript

f	fin
b	base

c	fin cross section
Y	Young's Contact Angle
t	total
o	overall
wall	wall

ACKNOWLEDGMENTS

This work was supported by National Research Foundation of Korea (NRF) grants funded by the Korean government (MSIP) (2014M2B2A9031122). This research was supported by Nano•Material Technology Development Program through the National Research Foundation of Korea(NRF) funded by the Ministry of Science, ICT and Future Planning.(2009-0082580)

REFERENCES

1. W. M. Rohsenow, "A method of correlating heat transfer data for surface boiling of liquids," *Trans. ASME*, **84**, 969 (1962)
2. N. Kurul, M.Z. Podowski, "Multidimensional effects in forced convection subcooled boiling," Proceedings of the 9th International Heat Transfer Conference, Jerusalem, Israel, pp. 21–25, 1990.
3. N. Zuber, "Hydrodynamic Aspect of Boiling Heat Transfer," AEC Report No. AECU-4439 (1968)
4. S. S. Kutateladze, "On the Transition to Film Boiling under Natural Convection," Kotloturbostroenie **3**, 10–12 (1948)
5. Y. Katto, and S. Yokoya, "Principal Mechanism of Boiling Crisis in Pool Boiling," Int. J. Heat Mass Tranfser **11**, 993 (1968)
6. Y. Haramura, and Y. Katto, , "New Hydrodynamic Model of Critical Heat Flux Applicable Widely to both Pool and Forced Convection Boiling on Submerged Bodies in Struated Liquids," Int. J. Heat Mass Transfer **26**, 379 (1983)
7. H. D. Kim and M. H., Kim "Effect of Nanoparticle Deposition on Capillary Wicking that Influences the Critical Heat Flux in nanofluids," Appl. Phys. Lett. **91**, 014104 (2007)
8. S. M. You, J. H. Kim and K. H. Kim, "Effect of nanoparticles on critical heat flux of water in pool boiling heat transfer," Applied Physics Letters, **83**, 3374 (2003)
9. I. C. Bang, J. Buongirno, L. W. Hu and H. Wang, "Measurement of Key Pool Boiling Parameters in Nanofluids for Nuclear Application," Journal of Power and Energy Systems, **2**, pp. 340-351 (2008)
10. R. Chen, M. C. Lu, V. Srinivasan, Z. Wang, H.H. Cho and A. Majumadar, "Nanowires for Enhanced Boiling Heat Transfer," Nano Lettes, **9**(2), pp 548-553, (2009)
11. H. J. Jo, S. H. Kim, H. Kim, J. Kim and M. H. Kim, "Nucleate boiling performance on nano / microstructures with different wetting surface," Nanoscaled Research Letters, **7**, 242 (2012)
12. S. G. Liter and M. Kaviany, "Pool-boiling CHF enhanced by modulated porous-layer coating: theory and experiment," Int. J. Heat Mass Transfer **44**(22), 4287 (2001)
13. S. G. Kandlikar, "A Theoretical Model to Predict Pool Boiling CHF Incorporating Effects of Contact Angle and Orientation," J. Heat Transfer **123**, pp. 1071–1079 (2001)
14. K. H. Chu, R. Enright, and E. N. Wang, "Structured surfaces for Enhanced Pool Boiling Heat Transfer," Appl. Phys. Lett. **100**(24), 241603 (2012)
15. F. P. Incropera, D. P. Dewitt, T. L. Bergman and A. S. Lavine, *Fundamentals of Heat and Mass Transfer (6th Edition)*, Wiley, USA (2007)
16. P.C. Carman, "Fluid Flow through Granular Beds," Transactions of the Inst. of Chem. Eng. **15**, 150–66 (1937)